

Liquid-solid and vapor-solid distributions of vapor-liquid-solid III-V ternary nanowires

Vladimir G. Dubrovskii*

Faculty of Physics, St. Petersburg State University, Universitetskaya Embankment 13B, 199034 St. Petersburg, Russia

 (Received 26 June 2023; revised 25 July 2023; accepted 24 August 2023; published 11 September 2023)

III-V ternary nanowires and nanowire heterostructures offer almost unlimited possibilities for the band-gap design and can be integrated with Si electronic platform. Most of such nanowires are grown by the vapor-liquid-solid method. The presence of a catalyst droplet, which is a quaternary liquid alloy for Au-catalyzed III-V ternary nanowires, significantly complicates the analysis of the nanowire composition versus the vapor and liquid compositions. Herein, we develop a growth theory of III-V ternary nanowires and obtain the stationary liquid-solid distribution in a rather general form. It is shown that the liquid-solid distribution is close to equilibrium, or nucleation limited, for nanowires based on group III intermix, and becomes kinetically controlled for nanowires based on group V intermix. These principally different behaviors are due to extremely low concentrations of highly volatile group V elements in a droplet, leading to group V limited liquid-solid growth. We also consider the vapor-solid distributions of III-V ternary nanowires and demonstrate that they are controlled by the material influxes into the droplet, and almost independent of the liquid composition in many cases, at least for ternaries based on group III intermix. The examples of the liquid-solid and vapor-solid distributions are given for different material systems including Au-catalyzed InGaAs and AlGaAs nanowires, and self-catalyzed InPAs, GaSbAs, and AlSbAs nanowires, which fit very well the available experimental data.

DOI: [10.1103/PhysRevMaterials.7.096001](https://doi.org/10.1103/PhysRevMaterials.7.096001)

I. INTRODUCTION

Compositional control over III-V ternary semiconductor materials and nanomaterials of different types is essential for the band-gap design and development of functional nanoheterostructures based on such materials [1–3]. III-V nanowires (NWs) and NW heterostructures are widely considered as fundamental building blocks for nanoscience and nanotechnology [4–7]. The lattice mismatch issue, which remains the most challenging bottleneck for fabrication of III-V heterostructures in highly mismatched material systems and dislocation-free planar growth of III-V materials on Si substrates, can be fully circumvented in the NW geometry due to a small contact area of the lattice-mismatched materials [8–10]. Therefore, III-V NWs offer almost unlimited possibilities for the bottom-up band-gap engineering and monolithic integration of photonic III-V nanoheterostructures with Si electronic platform [4–7]. The vapor-liquid-solid (VLS) growth with a metal catalyst particle [11] remains the most common method to fabricate semiconductor NWs by different epitaxy techniques. For the VLS growth of III-V NWs, a foreign catalyst metal (often Au) can be replaced with a group III metal in the self-catalyzed approach [12]. This allows one to safely avoid the unwanted Au contamination of NWs and tune the NW morphology by changing the droplet size during growth [13]. The rapid progress in the VLS growth, characterization, and functionalization techniques (see Refs. [4–7] for a detailed review) has been

accomplished with the advanced growth modeling of III-V NWs (see Ref. [13] for a recent review).

Compositions of III-V ternary NWs and NW heterostructures based on group III [14–25] and group V [26–37] intermix (interchange) have mainly been studied versus the technologically controlled vapor fluxes. For a ternary $A_xB_{1-x}C$ NWs based on intermix of the elements A and B , the vapor-solid distribution $x(z)$ relates the NW composition x to the fraction of A atoms in vapor, $z = I_A/(I_A + I_B)$, where I_A and I_B are the atomic fluxes of A and B species. In particular, it has been found that the vapor-solid distributions of NWs composed of highly mismatched binaries such as InGaAs [14–18], InGaN [25], and GaSbAs [34,35] show no thermodynamic miscibility gaps at the growth temperatures, suggesting that their VLS growth is controlled by the material inputs at relatively high supersaturations. The liquid-solid distribution $x(y)$, which relates the NW composition to the fraction of A atoms in the droplet, $y = \chi_A/(\chi_A + \chi_B)$, with χ_A and χ_B as the atomic concentrations of elements A and B in liquid, has been measured only once using *in situ* growth monitoring of Au-catalyzed InGaAs NWs at 380 °C [19]. The measured liquid-solid distribution of these InGaAs NWs had a nonlinear shape with a miscibility-gap region, which was fitted by a kinetic model [19].

While the liquid state may be unimportant for the vapor-solid distributions (see the discussion hereinafter), the liquid-solid distributions are essential for modeling the compositional profiles across axial NW heterostructures, influenced by the reservoir effect in a catalyst droplet [21,38]. Therefore, most theoretical works, reviewed in Refs. [38–40], studied the liquid-solid distributions of VLS III-V ternary NWs [41–50]. The liquid-solid growth models developed so

*dubrovskii@mail.ioffe.ru

far can be divided into the pure equilibrium model considering the equilibrium for AC and BC binaries in liquid and solid [21,41], the nucleation-limited model considering the composition of the critical nucleus [42–44], the simple kinetic approach neglecting the composition-dependent chemical potential of a ternary solid [22,45,46], and the advanced kinetic models considering the liquid-solid growth of fractional $A_xB_{1-x}C$ monolayer from a ternary $A-B-C$ or quaternary $A-B-C-Au$ liquid melt [19,47–50]. Much fewer models tried to link directly the NW composition to the vapor composition [22,25,45], and often resulted in the one-parametric Langmuir-McLean equation [51] for the stationary vapor-solid distribution [22,25]. The general kinetic approach developed in Ref. [52] for III-V ternary materials based on group III intermix grown under low III/V flux ratios, and in Ref. [53] for any III-V ternary materials under arbitrary III/V flux ratios, treated the vapor-solid distributions $x(z)$. Although successfully applied to VLS III-V ternary NWs, the models of Refs. [52,53] did not consider explicitly a liquid droplet at the NW top and the complex interplay between the liquid-solid growth of NW monolayers and the vapor-liquid material exchange at the droplet surface, including the diffusion fluxes of group III adatoms.

It should be noted that the presence of a liquid droplet on top of III-V ternary NWs significantly complicates the compositional modeling. Indeed, in the most general case of Au-catalyzed VLS growth, quaternary liquid alloy is characterized by the three atomic concentrations χ_A , χ_B and χ_C (with $\chi_{Au} = 1 - \chi_A - \chi_B - \chi_C$), and is described by complex chemical potentials of A , B , and C elements which include interactions between different atoms [38–44,47–50]. While the fractions of group III atoms in the droplet can be measured during [19] or after [13,21,28] NW growth, it is principally impossible to access the extremely low concentrations of highly volatile group V atoms such as As, P, or N. Therefore, it is highly desirable to circumvent the uncertainty in the unknown group V concentration in the droplet, which is absent in the nucleation-limited [42–44] but present in the kinetic [19,47,48,50] liquid-solid distribution. Furthermore, the kinetic approach of Ref. [47] and its further generalizations were based on the binary growth model in which A , B and C atoms are attached to a growing island as AC and BC pairs. This assumption is generally wrong for the attachment processes from nonstoichiometric liquid, and can be used only approximately under C -rich growth conditions [52]. Rather, A , B , and C atoms are attached in such a way that the total number of the attached A and B atoms equals the total number of the attached C atoms to ensure that the solid alloy is stoichiometric. This important difference, known for the vapor-solid growth of $InSb_xAs_{1-x}$ epilayers from the seminal work of Biefeld [2], was accounted for in Ref. [53], and resulted in the vapor-solid distribution which depends on the total flux ratio $\varepsilon_g = (I_A + I_B)/I_C$, with I_C as the atomic vapor flux of C species. It has been shown that C -rich growth of a ternary based on A and B intermix at $\varepsilon_g \ll 1$ leads to the kinetically controlled composition, while it becomes close to equilibrium under C -poor conditions at $\varepsilon_g \gg 1$ [53].

In this work, we use the approach of Ref. [53] for the liquid-solid growth of III-V ternary islands of VLS NWs. The growth of single-NW monolayer in liquid is consid-

ered using the diffusion fluxes in multicomponent systems expressed through activities of different atoms [54]. The obtained liquid-solid distribution shows the general properties predicted in Ref. [53]. The liquid droplets in Au-catalyzed and self-catalyzed VLS growth are group-III rich and group-V poor regardless of the growth conditions. Consequently, the liquid-solid distribution is kinetically controlled for VLS ternary NWs based on group V intermix, and is reduced to the earlier result [47,50] with the decrypted kinetic parameter. For VLS ternary NWs based on group III intermix, the situation is reversed and the liquid-solid distribution becomes close to equilibrium, or nucleation-limited shape [43,44]. These equilibrium and nucleation-limited models yield the same result for the $x(y)$ dependence, which is independent of the unknown group V concentration χ_5 in the nucleation-limited model [43,44], while in the equilibrium model the χ_5 value is precisely determined as a function of the solid composition x [40,41]. We also analyze the vapor-solid distributions of VLS ternary NWs and show that the $x(z)$ dependence for group III intermix may be independent of the liquid state and fully determined by the material influxes of A and B atoms into the droplet. This yields the kinetic Langmuir-McLean vapor-solid distribution, observed earlier for VLS AlGaAs [22] and InGaN [25] NWs, whose shape is very different from the equilibrium distribution. We consider particular examples including Au-catalyzed In_xGaAs and AlGaAs NWs and self-catalyzed InPAs, GaSbAs, and AlSbAs NWs, and demonstrate a good correlation of the model with the available data.

II. LIQUID-SOLID DISTRIBUTIONS

Solid state in a III-V ternary $A_xB_{1-x}C$ NW is described by the chemical potentials of AC and BC pairs in the regular solid-solution model [40,41,43,44,47,48,50,52,53], given by

$$\begin{aligned}\mu_{AC} &= \mu_{AC}^0 + \ln x + \omega(1-x)^2, \\ \mu_{BC} &= \mu_{BC}^0 + \ln(1-x) + \omega x^2.\end{aligned}\quad (1)$$

Here and below, we express all the chemical potentials and binary interaction parameters in thermal units of $k_B T$, with T as the absolute temperature and k_B as the Boltzmann constant. The chemical potentials μ_{AC}^0 and μ_{BC}^0 correspond to solid binaries AC and BC , respectively, whereas ω is the binary (or pseudobinary) AC - BC interaction parameter in solid, which may be x dependent [44]. The corresponding activities of AC and BC pairs in solid, given by

$$\begin{aligned}\alpha_{AC} &= e^{\mu_{AC}} = e^{\mu_{AC}^0} x e^{\omega(1-x)^2}, \\ \alpha_{BC} &= e^{\mu_{BC}} = e^{\mu_{BC}^0} (1-x) e^{\omega x^2},\end{aligned}\quad (2)$$

determine the rejected material fluxes in the kinetic equation for the growth rate of a ternary island from liquid [47]. The attachment rates for AC and BC binaries are introduced empirically in the existing kinetic models [40,47,50], and do not include any atomic details of the diffusion processes in liquid.

To go beyond this approach, we introduce the normalized diffusion fluxes at the liquid-solid interface under the droplet (measured in s^{-1}) of a multicomponent liquid according to

Ref. [54]:

$$\mathbf{j} = -\frac{De^{-\mu_0}}{\Omega_l^{2/3}} \nabla \alpha, \quad \alpha = e^\mu. \quad (3)$$

Here, α is the activity of a given element with the chemical potential μ (which depends on the three atomic concentrations in a quaternary liquid), μ_0 is the reference chemical potential corresponding to pure liquid of this element, D is the diffusion coefficient, and Ω_l is the average volume per atom in liquid. For perfect solution without interactions, we simply have $\mu = \mu_0 + \ln \chi$, and Eq. (3) is reduced to the standard diffusion flux $\mathbf{j} = -D\nabla n$, with $n = \chi/\Omega_l^{2/3}$ as the surface concentration at the liquid-solid interface. For a quaternary A - B - C -Au liquid, the diffusion fluxes of A , B , and C atoms are therefore given by

$$\mathbf{j}_k = -d_k \nabla \alpha_k, \quad d_k = \frac{D_k e^{-\mu_{k,0}}}{\Omega_l^{2/3}}, \quad k = A, B, C, \quad (4)$$

with the atomic concentrations χ_k and the corresponding activities in liquid α_k :

$$\alpha_k = e^{\mu_k} = e^{\mu_k^0 + \psi_k} \chi_k, \quad k = A, B, C. \quad (5)$$

Here, μ_k^0 are the chemical potentials in pure liquids, and ψ_k are the interaction terms of the chemical potentials $\mu_k = \mu_k^0 + \ln \chi_k + \psi_k$ of atoms $k = A, B, C$ [40,44,50]. Since we consider a solution of A , B , and C atoms in Au, D_k in Eq. (4) should correspond to the diffusion coefficients of these atoms in liquid Au at a given temperature. For the self-catalyzed VLS growth of III-V ternary NWs without any Au, these D_k s describe the diffusivities of group V atoms and the minority group III atoms (such as Al in pure Ga droplet for AlGaC NWs [21] and Ga in pure In droplet for InGaC NWs [25,43]).

The growth model of a ternary island (or fractional monolayer) in a VLS NW is illustrated in Fig. 1. We assume that the diffusion fluxes of A , B , and C atoms are directed along the liquid-solid interface under the droplet into the island boundary. The activities of A , B , and C atoms become spatially uniform at a distance Λ from the island boundary in contact with liquid, with Λ as the characteristic length of inhomogeneity of a liquid alloy, which is much smaller than the island radius R . This corresponds to the ballistic regime of two-dimensional liquid-solid growth [47,55,56]. Since there are no sources or sinks of atoms over the distance Λ , the diffusion equations for the coordinate-dependent activities $\tilde{\alpha}_k$ are simply given by

$$\frac{d^2 \tilde{\alpha}_k}{d\xi^2} = 0, \quad k = A, B, C, \quad (6)$$

where ξ is the distance from the island boundary ($0 \leq \xi \leq \Lambda$). From Eq. (6), the three $\tilde{\alpha}_k$ s are linear functions of ξ , with two unknown constants each. To determine the six constants, we use the boundary conditions away from the island boundary (at $\xi = \Lambda$)

$$\tilde{\alpha}_k(\xi = \Lambda) = \alpha_k, \quad k = A, B, C, \quad (7)$$

according to the ballistic growth model with a constant island “feeding zone” of width Λ [55,56]. At the island boundary, the products of the liquid activities of A - C and B - C pairs of

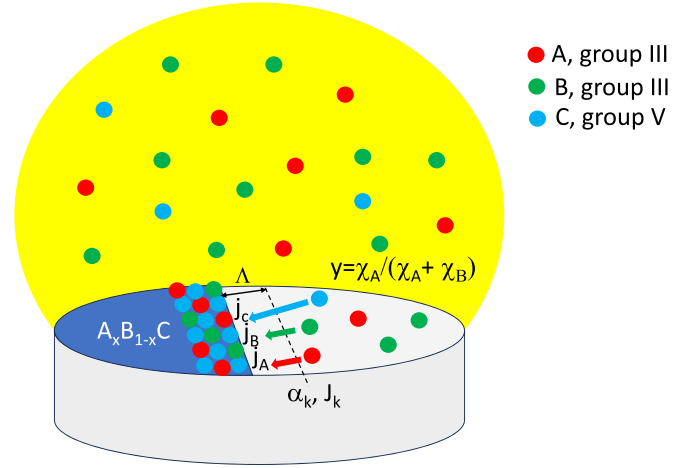


FIG. 1. Illustration of liquid-solid growth model for ternary island (fractional monolayer) $A_x B_{1-x} C$ based on group III intermix. Quaternary A - B - C -Au liquid in droplet is C poor. Diffusion fluxes j_A , j_B , and j_C are directed along liquid-solid interface under droplet into island, with $j_A + j_B = j_C$ to ensure that solid alloy is stoichiometric. Incoming fluxes at distance Λ from island boundary equal J_A , J_B , and J_C , and spatially uniform activities equal α_A , α_B , and α_C . Due to $\chi_C \ll \chi_A + \chi_B$, most A and B atoms must be rejected from island boundary, because they cannot crystallize in absence of C atoms available for stoichiometric growth.

atoms should equal to the activities of AC and BC pairs in pseudobinary solid:

$$\begin{aligned} \tilde{\alpha}_A(\xi = 0) \tilde{\alpha}_C(\xi = 0) &= \alpha_{AC}, \\ \tilde{\alpha}_B(\xi = 0) \tilde{\alpha}_C(\xi = 0) &= \alpha_{BC}, \end{aligned} \quad (8)$$

as in Ref. [53] for the vapor-solid growth. Atoms from liquid do not join the island in pairs. Equation (8) states that the products of the two activities $\tilde{\alpha}_A \tilde{\alpha}_C$ and $\tilde{\alpha}_B \tilde{\alpha}_C$ become equal to the activities of AC and BC pairs in solid, α_{AC} and α_{BC} at the island boundary, as in the growth models of Refs. [40,47,52] but beyond the assumption of C -rich growth (in which case $\tilde{\alpha}_C$ can be treated as a spatially independent constant [52]). According to Eqs. (7) and (8), the activities of atoms A , B , and C in liquid change from the spatially independent α_k at the distance Λ from the island boundary to those given by Eq. (8) at the island boundary (over the distance Λ , which is much smaller than the linear island size). It is possible that the characteristic lengths are different for different atoms, in which case Eq. (7) changes to $\tilde{\alpha}_k(\xi = \Lambda_k) = \alpha_k$ for $k = A, B, C$. This does not affect the final results for the diffusion fluxes feeding the island.

Finally, the diffusion fluxes

$$j_k = \left. \frac{d\tilde{\alpha}_k}{d\xi} \right|_{\xi=0}, \quad k = A, B, C \quad (9)$$

must obey

$$j_A + j_B = j_C. \quad (10)$$

to ensure that the NW is stoichiometric, as in Ref. [53]. The growth rates of the numbers of AC and BC pairs in the island, N_A and N_B , and the total growth rate of the island, considered

in Refs. [47–50,56], are given by

$$\frac{dN_A}{dt} = 2Pj_A, \quad \frac{dN_B}{dt} = 2Pj_B, \quad \frac{dN_A}{dt} + \frac{dN_B}{dt} = 2Pj_C, \quad (11)$$

where P is a time-dependent length of the island boundary in contact with liquid. The coefficient 2 accounts for the two diffusion fluxes incorporating into the island boundary from the liquid-solid interface around the island and from its top. These equations are, however, different from Refs. [47–50,56] due to the additional condition $j_A + j_B = j_C$, while the prior works considered only the fluxes of A and B atoms. This indirectly implied that a catalyst droplet is C rich and the liquid-solid growth is limited by the diffusion fluxes of A and B atoms. In our approach, the sum of A and B diffusion fluxes into the island must equal the diffusion flux of C atoms. For a ternary NW based on group III intermix, illustrated in Fig. 1, the droplet is C poor. Most group III atoms present in the droplet cannot enter the island due to insufficient amount of group III atoms. Hence, a significant fraction of the incoming group III diffusion fluxes should be rejected by the island. For a ternary NW based on group V intermix, the droplet is C rich. In this case, almost all A and B atoms diffusing to the island boundary should be incorporated into the NW, and the liquid-solid growth is indeed limited by the diffusion fluxes of A and B atoms.

The five boundary conditions given by Eqs. (7) and (8) lead to the following nonlinear system of algebraic equations for the diffusion fluxes j_A , j_B , and j_C :

$$(J_A - j_A)(J_C - j_C) = F_A, \quad (12)$$

$$(J_B - j_B)(J_C - j_C) = F_B, \quad (13)$$

together with the sixth boundary condition given by Eq. (10). Here,

$$J_k = \frac{d_k \alpha_k}{\Lambda}, \quad k = A, B, C \quad (14)$$

are the incoming diffusion fluxes at the distance Λ from the island boundary, and

$$F_A = \frac{d_A d_C}{\Lambda^2} \alpha_{AC}, \quad F_B = \frac{d_B d_C}{\Lambda^2} \alpha_{BC} \quad (15)$$

are the functions describing interactions in a ternary solid and the corresponding rejected fluxes. The activities of AC and BC pairs in solid are given by Eq. (2).

The nonlinear system of Eqs. (12), (13), and (10) has the same form as in Ref. [53] for the vapor-solid growth. Its solution is given by

$$j_C = (J_A + J_B)G, \quad G = \frac{1}{2} \frac{(1 + \varepsilon_l)}{\varepsilon_l} \left[1 - \sqrt{1 - \frac{4\varepsilon_l \varphi}{(1 + \varepsilon_l)^2}} \right]. \quad (16)$$

$$j_A = \frac{j_C + j_*}{1 + F_B/F_A}, \quad j_B = \frac{(F_B/F_A)j_C - j_*}{1 + F_B/F_A}, \quad j_* = \frac{F_B}{F_A} J_A - J_B. \quad (17)$$

Here, the two important parameters of our theory are defined as follows:

$$\varepsilon_l = \frac{J_A + J_B}{J_C}, \quad (18)$$

$$\varphi = 1 - \frac{F_A + F_B}{(J_A + J_B)J_C}. \quad (19)$$

The parameter ε_l determines the ratio of the total incoming flux of A and B atoms over the incoming flux of C atoms. The parameter φ ($0 \leq \varphi \leq 1$) is related to the supersaturation level in a quaternary liquid with respect to a ternary solid, with $\varphi = 0$ corresponding to the no-growth equilibrium condition and $\varphi = 1$ to the liquid-solid growth at infinitely high supersaturation. Clearly, the solid composition of a ternary $A_x B_{1-x} C$ island is determined by

$$x = \frac{j_A}{j_A + j_B} = \frac{j_A}{j_C}. \quad (20)$$

This is equivalent to $x = dN_A/dt / (dN_A/dt + dN_B/dt)$, as in Ref. [47], because a time-dependent P cancels in the ratio of the two growth rates.

Introducing the effective liquid composition according to

$$Y = \frac{J_A}{J_A + J_B} \quad (21)$$

and using Eqs. (16) and (17), we arrive at the general liquid-solid distribution of the form

$$Y = \frac{1}{1 + F_B/F_A} (1 - G) + xG. \quad (22)$$

Here,

$$F_B/F_A = f(x)/c_l,$$

$$f(x) = \beta_l \frac{(1-x)}{x} e^{\omega(2x-1)}, \quad \beta_l = e^{\Delta\mu_{AC}^0 - \Delta\mu_{BC}^0 + \psi_A - \psi_B}, \quad (23)$$

and c_l is the kinetic constant given by

$$c_l = \frac{D_A}{D_B} e^{\psi_A - \psi_B}. \quad (24)$$

The liquid-solid distribution given by Eq. (22) is the main result of this work, which will be analyzed in detail in the next section. However, the main result is already seen from Eq. (22). The function $1/(1 + F_B/F_A) = 1/[1 + f(x)/c_l]$ is related to the equilibrium, or nucleation-limited distribution [41–44], and enters the general distribution with the weight $1-G$. According to Eq. (16) for G , this weight is very close to unity at $\varepsilon_l \gg 1$, that is, for group III intermix. Therefore, the liquid-solid distribution of VLS ternary NWs based on group III intermix is controlled by thermodynamics. For group V intermix at $\varepsilon_l \ll 1$, we have $G \cong \varphi$. This yields a kinetically controlled liquid-solid distribution, where thermodynamic factors become almost negligible at high liquid supersaturations (corresponding to $\varphi \rightarrow 1$). In this case, the liquid-solid distribution is reduced to $Y = x$.

The parameter ε_l , which determines the shape of the liquid-solid distribution, is similar to the total ratio of the vapor fluxes ε_g in Ref. [53]. However, there is one important difference. Considering ternaries based on group V intermix, the total V/III flux ratio can vary from ~ 1 to very large values on the order of 10–100, and is easily controlled in any epitaxy

technique. Increasing the V/III flux ratio leads to a transition from the kinetically controlled regime with an almost linear $x(z)$ dependence to the nucleation-limited composition with the miscibility gaps [2,53]. In VLS growth of III-V NWs, the situation is much simpler because the catalyst droplets contain a negligible amount of highly volatile As, P, or N atoms on the order of 0.01 [13] (with a probable exception of Sb [37]) regardless of the epitaxy technique, droplet size, vapor fluxes, and the presence or absence of Au in a droplet. Therefore, $\varepsilon_l \gg 1$ for most VLS NWs based on group III intermix and $\varepsilon_l \ll 1$ for all VLS NWs based on group V intermix, with almost no intermediate values of $\varepsilon_l \sim 1$ (which is the most common case for the vapor-solid growth). This fact considerably simplifies the analysis of the liquid-solid distributions of VLS III-V ternary NWs, and will be used in what follows.

III. ANALYSIS OF THE LIQUID-SOLID DISTRIBUTIONS

Using the definition of the effective liquid composition given by Eq. (21) and the fluxes J_A and J_B given by Eq. (14) with the activities in liquid defined in Eq. (5), Y is related to the actual liquid composition $y = \chi_A/(\chi_A + \chi_B)$ according to

$$Y = \frac{c_l y}{c_l y + 1 - y}, \quad (25)$$

with c_l given by Eq. (24). Using the same expressions in Eq. (18), we obtain

$$\varepsilon_l = \varepsilon(c_l y + 1 - y), \quad \varepsilon = \frac{D_B}{D_C} e^{\psi_B - \psi_C} \frac{\chi_{\text{tot}}}{\chi_C}, \quad (26)$$

where ε is the actual control parameter that determines the weights of the equilibrium versus kinetic liquid-solid distributions. From Eqs. (19), (15), and (2) it follows that

$$\varphi = 1 - \frac{\Gamma_l [c_l x e^{\omega(1-x)^2} + \beta_l (1-x) e^{\omega x^2}]}{c_l y + 1 - y}, \quad (27)$$

$$\Gamma_l = \frac{1}{\chi_{\text{tot}} \chi_C} e^{-\Delta\mu_{AC}^0 - \psi_A - \psi_C},$$

with Γ_l as the parameter that determines the level of liquid supersaturation. The control parameter ε contains three multiplying factors: the ratio of the diffusion coefficients of B over C atoms, the factor $\exp(\psi_B - \psi_C)$, and the ratio of the total concentration of A and B atoms $\chi_{\text{tot}} = \chi_A + \chi_B$ over the concentration of C atoms χ_C , which is on the order of 0.01 if A and B belong to group V. Considering self-catalyzed NWs based on group V intermix and neglecting small terms containing interaction with group V atoms in the regular solution model [43,46], we have $\psi_C \cong 0$, while ψ_B approximately equals the interaction parameter of B and C atoms in liquid. Using the data of Ref. [57] for $\psi_B - \psi_C \cong \omega_{BC}$, $\omega_{BC} = \omega_{\text{InAs}} = -4.00$ for $\text{In}_x\text{As}_{1-x}$ ternaries at 450 °C, $\omega_{BC} = \omega_{\text{GaAs}} = -4.49$ for $\text{Ga}_x\text{As}_{1-x}$ ternaries at 500 °C, and $\omega_{BC} = \omega_{\text{AlAs}} = -6.27$ for $\text{Al}_x\text{As}_{1-x}$ ternaries at 600 °C. These examples show that the ε value is even smaller than 0.01, which is why the limiting behavior of $\varepsilon \rightarrow 0$ should be a good approximation for the liquid-solid distribution of ternaries based on group III intermix in nearly all cases. For self-catalyzed $\text{In}_x\text{Ga}_{1-x}\text{As}$ NWs with $B = \text{Ga}$ and $C = \text{As}$, Ga, and As atoms in pure In droplet interact only with In atoms, which is why $\psi_B - \psi_C \cong$

$\omega_{AB} - \omega_{AC} = \omega_{\text{InGa}} - \omega_{\text{InAs}}$. This difference is positive and equals 4.88 at 450 °C [57]. Therefore, the ε parameter is around $(D_{\text{Ga}}/D_{\text{As}}) \times 10^4$, and even if As is a slower diffuser in liquid In compared to Ga, the ε value should be much larger than unity. However, the situation changes dramatically when Ga and As diffuse in pure Au, where $\psi_B - \psi_C \cong \omega_{\text{AuGa}} - \omega_{\text{AuAs}} = -8.45$ at 450 °C [46]. For a Au-In alloy with 50% composition, we have $\psi_B - \psi_C \cong -1.78$ and the ε value decreases to $\sim (D_{\text{Ga}}/D_{\text{As}}) \times 17$. Similar analysis shows that very high values of $\varepsilon > 100$ are guaranteed for all self-catalyzed $\text{In}_x\text{Ga}_{1-x}\text{As}$ and $\text{Ga}_{1-x}\text{Al}_x\text{As}$, and all VLS $\text{In}_x\text{Ga}_{1-x}\text{P}$ and $\text{Ga}_{1-x}\text{Al}_x\text{P}$ NWs. The presence of Au in the droplets of InGaAs and GaAlAs NWs may reduce the ε values to ~ 10 at $\chi_{\text{Au}} \sim 0.5$. Nevertheless, the limiting cases of $\varepsilon \ll 1$ for group V intermix and $\varepsilon \gg 1$ for group III intermix should work well in most cases.

The purely kinetic distribution at $\varepsilon \rightarrow 0$, which applies to group V intermixes, is obtained from Eq. (22) at $G = \varphi$ in the form

$$y = \frac{x + g(x)}{c_l + (1 - c_l)x}, \quad g(x) = (1-x)x\Gamma_l [c_l e^{\omega(1-x)^2} - \beta_l e^{\omega x^2}]. \quad (28)$$

This liquid-solid distribution is identical to the result of Refs. [47–50], where the kinetic parameter c_l was not determined. Neglecting again the small c_5 and c_5^2 terms in the regular solution model, Eq. (28) is simplified to

$$y = \frac{x}{c_l + (1 - c_l)x} [1 + \Gamma_l (1-x) (c_l e^{\omega(1-x)^2} - \beta_l e^{\omega x^2})],$$

$$c_l = \frac{D_A}{D_B} \delta(\chi_3), \quad \beta_l = e^{\Delta\mu_{AC}^0 - \Delta\mu_{BC}^0} \delta(\chi_3),$$

$$\delta(\chi_3) = \exp[(\omega_{3A} - \omega_{3B})\chi_3 + (\omega_{\text{AuA}} - \omega_{\text{AuB}})(1 - \chi_3)],$$

$$\Gamma_l = \frac{1}{\chi_{\text{tot}} \chi_3} \frac{e^{-\Delta\mu_{AC}^0}}{f_A(\chi_3)},$$

$$f_A(\chi_3) = \exp[\omega_{3A}\chi_3 + \{\omega_{\text{AuA}} + \omega_{3\text{Au}}(1 - 2\chi_3)\}(1 - \chi_3)], \quad (29)$$

with ω_{ik} as the binary interaction parameters in liquid in the regular solution model [43,44]. Importantly, the parameters c_l , β_l , and Γ_l on the right-hand side are independent of y and depend only on the concentration of group III atoms in the droplet χ_3 (or, equivalently, Au atoms due to $\chi_{\text{Au}} \cong 1 - \chi_3$). Therefore, the right-hand side is a function of x only, and Eqs. (29) provides explicitly the liquid-solid distribution in the form of $y(x)$ dependence.

The equilibrium distribution at $\varepsilon \rightarrow \infty$, which applies to group III intermixes, corresponds to $G = 0$ in Eq. (22). Using Eq. (25), the liquid-solid distribution becomes

$$y = \frac{1}{1 + f(x)}, \quad (30)$$

with $f(x)$ given by Eq. (23). This result is identical to the nucleation-limited model of Refs. [43,44], where it was shown that the right-hand side is independent of y for most self-catalyzed [43] and many Au-catalyzed [44] VLS NWs. The analysis of Refs. [43,44] fully applies to ternaries based on group III intermix, but not to group V intermix. One

important conclusion is that the equilibrium distribution is almost independent of the concentration of a third group V element χ_C [43].

It is interesting to note that the limiting case of $\varepsilon \rightarrow \infty$ yielding $G = 0$ is equivalent to the true equilibrium at $\varphi = 0$, which results in $G = 0$ for any ε according to Eq. (16). Under the equilibrium conditions, we have $j_C = 0$ from Eq. (16). This should correspond to $j_A = 0$, $j_B = 0$ and not $j_A + j_B = 0$, because all three fluxes must cancel at equilibrium. From Eq. (17), the flux j_* must be zero, which yields the equilibrium conditions of the form $\alpha_A\alpha_C = \alpha_{AC}$ and $\alpha_B\alpha_C = \alpha_{BC}$, or

$$\mu_A + \mu_C = \mu_{AC}, \quad \mu_B + \mu_C = \mu_{BC}, \quad (31)$$

as previously considered in Ref. [41]. These equilibrium conditions give the same liquid-solid distribution as the nucleation-limited model [43], which is given by Eq. (30). As mentioned above, the only difference between the nucleation-limited and equilibrium approaches is in the concentration of a third element C. The value of χ_C remains undetermined in the nucleation-limited model, while the equilibrium model provides χ_C in the form [40]

$$\chi_C = \frac{x}{\chi_{\text{tot}}y} e^{-\Delta\mu_{AC}^0 - \psi_A - \psi_C} e^{\omega(1-x)^2}. \quad (32)$$

Due to $\varepsilon \ll 1$ for group V intermix and $\varepsilon \gg 1$ for group III intermix, the approximation

$$G = \frac{\varphi}{1 + \varepsilon_l} \quad (33)$$

works well in all cases. Using Eqs. (22), (23), and (25)–(27), it is easy to obtain the general liquid-solid distribution in the form of nonlinear combination of the equilibrium and kinetic distributions [53]:

$$y(x) = \frac{t(x) - 1}{c_l - 1}, \quad t(x) = \begin{cases} \frac{a(x)}{2} [1 - \sqrt{1 + 4b(x)}], & a \leq 0 \\ \frac{a(x)}{2} [1 + \sqrt{1 + 4b(x)}], & a > 0 \end{cases}$$

$$a(x) = \left[\frac{1 + f(x)/c_l}{1 + f(x)} \right] \frac{(c_l - 1)x + c_l(\varepsilon - 1)}{\varepsilon},$$

$$b(x) = \varepsilon \left[\frac{1 + f(x)}{1 + f(x)/c_l} \right] \frac{(c_l - 1)g(x) + c_l}{[(c_l - 1)x + c_l(\varepsilon - 1)]^2}. \quad (34)$$

These expressions are reduced to the purely kinetic distribution given by Eq. (28) at $\varepsilon \rightarrow 0$ and to the equilibrium distribution given by Eq. (30) at $\varepsilon \rightarrow \infty$. For practical purposes, one can use the linear interpolation

$$y = \frac{1}{1 + f(x)} \frac{\varepsilon}{1 + \varepsilon} + \frac{x + g(x)}{c_l + (1 - c_l)x} \frac{1}{1 + \varepsilon}, \quad (35)$$

where the equilibrium and kinetic distributions enter the general liquid-solid distributions with the weights $\varepsilon/(1 + \varepsilon)$ and $1/(1 + \varepsilon)$, respectively. Figure 2 shows the vapor-solid distributions obtained from Eq. (34) for a hypothetical VLS system at a fixed $\omega = 2.3$, $\beta_l = 0.1$, $\Gamma_l = 0.2$, and $c_l = 3$, which are almost indistinguishable from the curves given by the simplified Eq. (35). As expected, the distribution is very close to the kinetic curve at a small ε of 0.05, and to the equilibrium curve at a large ε of 20. The miscibility-gap region, present in the equilibrium liquid-solid distribution, remains for group III intermix but is fully circumvented for group V intermix.

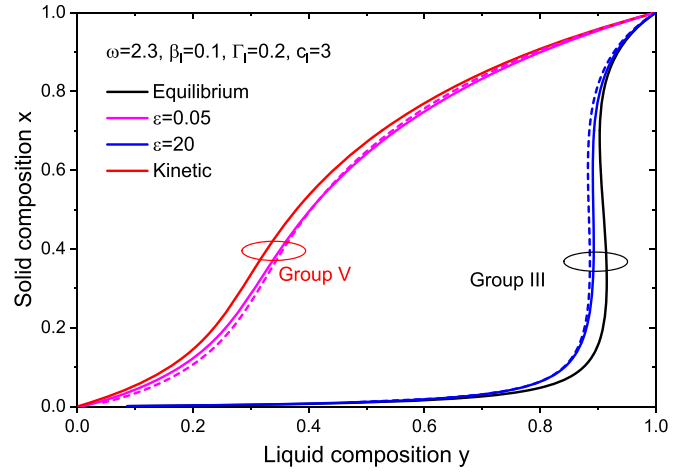


FIG. 2. Liquid-solid distributions for VLS NW at a fixed $\omega = 2.3$, $\beta_l = 0.1$, $\Gamma_l = 0.2$, and $c_l = 3$. All possible shapes, accessible by varying ε parameter, are restricted by equilibrium distribution containing miscibility gap due to $\omega > 2$, and smooth kinetic distribution. At small ε of 0.05, distribution for group V intermix is very close to kinetic shape. At large ε of 20, distribution for group III intermix is near equilibrium, and also contains miscibility gap. Solid curves are obtained from Eq. (34), and very well fitted by approximate Eq. (35) (dashed lines).

Figure 3 shows the liquid-solid distribution of $\text{In}_x\text{Ga}_{1-x}\text{As}$ NWs grown by Au-catalyzed metalorganic vapor-phase epitaxy (MOVPE) at 380°C , obtained in Ref. [19] using *in situ* monitoring inside a transmission electron microscope. The NWs were obtained using 30-nm-diameter colloidal Au nanoparticles, under a gas-phase V/III ratio of 1000 and variable fluxes of In and Ga precursors. The Au concentration in In-Ga-As-Au droplet was estimated at $\chi_{\text{Au}} = 0.57$. It is seen that the measured liquid-solid distribution shows a nonlinear behavior which is close to the equilibrium shape. The equilibrium curve was obtained from Eqs. (30) and (23) using the

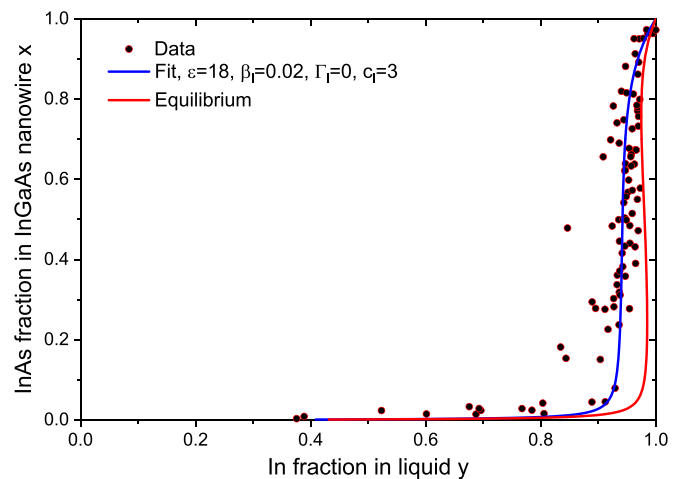


FIG. 3. Liquid-solid distribution of $\text{In}_x\text{Ga}_{1-x}\text{As}$ NWs grown by Au-catalyzed MOVPE at 380°C (symbols), fitted by Eq. (35) with parameters given in legend (blue line). Red line shows equilibrium distribution with miscibility gap at $\omega = 2.724$.

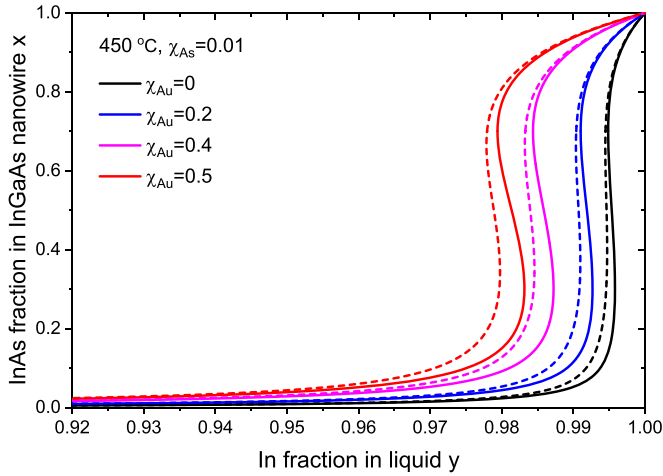


FIG. 4. Liquid-solid distributions of $\text{In}_x\text{Ga}_{1-x}\text{As}$ NWs at 450°C at fixed As concentration of 0.01 and different Au concentrations shown in legend. Solid lines correspond to equilibrium distributions. Dashed lines show general distributions affected by kinetic factors, which have a little influence on distribution shapes in all cases.

regular solution model at a fixed $\chi_{\text{Au}} = 0.57$ with the parameters of In-Ga-As-Au system given in Ref. [40]. In particular, a small β_l value of ~ 0.02 yields very high In concentrations in the droplet compared to Ga, as in Refs. [43,44]. A large binary interaction constant $\omega = 2.724$ yields the wide miscibility gap at 380°C , and corresponds to an almost vertical part of the measured $x(y)$ dependence for x from ~ 0.2 to ~ 0.8 . The nonlinear liquid-solid distribution is well fitted by Eq. (35) with $g(x) = 0$. This corresponds to $\Gamma_l \rightarrow 0$ in Eq. (28). At $\beta_l \ll 1$, the function $g(x)$ is proportional to $\Gamma_l c_l = \exp(-\Delta\mu_{\text{InAs}}^0 - \psi_{\text{Ga}} - \psi_{\text{As}})/(\chi_{\text{tot}}\chi_{\text{As}})$, which is less than 0.1 for $\chi_{\text{As}} > 0.01$ according to our estimates. Figure 4 shows the calculated equilibrium liquid-solid distributions of Au-catalyzed $\text{In}_x\text{Ga}_{1-x}\text{As}$ NWs at 450°C (corresponding to $\omega = 2.375$) for different Au concentrations from 0 to 0.5, compared to the general distribution obtained from Eqs. (35), (28), (23), and (24) at a fixed $\chi_{\text{As}} = 0.01$ using the regular solution model with the parameters of Ref. [40]. The equilibrium curves are almost the same as in Ref. [44] and show that the In fraction in the droplet y required to obtain any appreciable amount of InAs in NWs slightly decreases with increasing χ_{Au} , while the miscibility gap slightly narrows. The general curves are close to equilibrium in all cases. However, the miscibility-gap suppression is more probable in self-catalyzed NWs at $\chi_{\text{Au}} = 0$ and generally for smaller Au concentrations in the droplets.

Figure 5 shows the kinetic liquid-solid distributions of self-catalyzed $\text{InP}_x\text{As}_{1-x}$ NWs at 450°C , obtained from Eq. (29) at different total concentrations of group V atoms from 0.003 to 0.03. The parameters of the system are the same as in Ref. [46]: $\omega = 0.485$, $\omega_{\text{InP}} = 1.13$, $\omega_{\text{InAs}} = -4.00$, $\Delta\mu_{\text{InAs}}^0 = 8.65$, and $\Delta\mu_{\text{InP}}^0 = 7.495$. In calculations, we assumed that $D_{\text{P}}/D_{\text{As}} = 1$. This material system is characterized by relatively small interactions of dissimilar III-V pairs in solid, which is why the kinetic distributions are not very different from the equilibrium shape. The parameter Γ_l tends to zero at $\chi_{\text{tot}} > 0.03$, where the kinetic distributions saturate

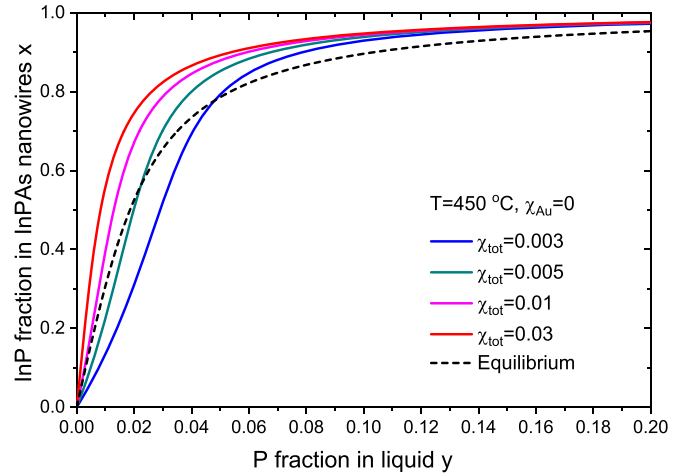


FIG. 5. Liquid-solid distributions of self-catalyzed $\text{InP}_x\text{As}_{1-x}$ NWs at 450°C , obtained from Eq. (29) at different total concentrations of group V atoms shown in legend. Dashed line shows equilibrium distribution obtained from Eqs. (30) and (23), which is same as in Ref. [46].

to the purely kinetic Langmuir-McLean curve. The situation changes for material systems with strong interactions between dissimilar III-V pairs, particularly antimonides. Figure 6 shows the kinetic liquid-solid distributions of self-catalyzed $\text{AlSb}_x\text{As}_{1-x}$ NWs at 600°C , obtained from Eq. (29) at different total concentrations of group V atoms from 0.004 to 0.03, with the parameters of Refs. [57,58]: $\omega = 2.215$, $\omega_{\text{AlSb}} = -1.92$, $\omega_{\text{AlAs}} = -6.27$, $\Delta\mu_{\text{AlSb}}^0 = 7.96$, and $\Delta\mu_{\text{AlAs}}^0 = 15.96$, assuming $D_{\text{Sb}}/D_{\text{As}} = 1$. All these curves are far from equilibrium and approach the purely kinetic Langmuir-McLean curve at large enough $\chi_{\text{tot}} > 0.03$. The miscibility gap, present in the equilibrium distribution and in the general distributions

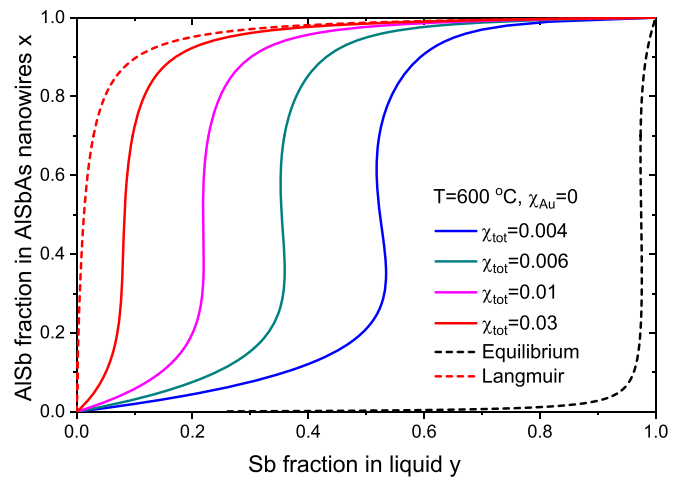


FIG. 6. Liquid-solid distributions of self-catalyzed $\text{AlSb}_x\text{As}_{1-x}$ NWs at 600°C , obtained from Eq. (29) at different total concentrations of group V atoms shown in legend. Black dashed line shows equilibrium distribution obtained from Eqs. (30) and (23). Red dashed line corresponds to purely kinetic Langmuir-McLean curve at $\Gamma_l = 0$.

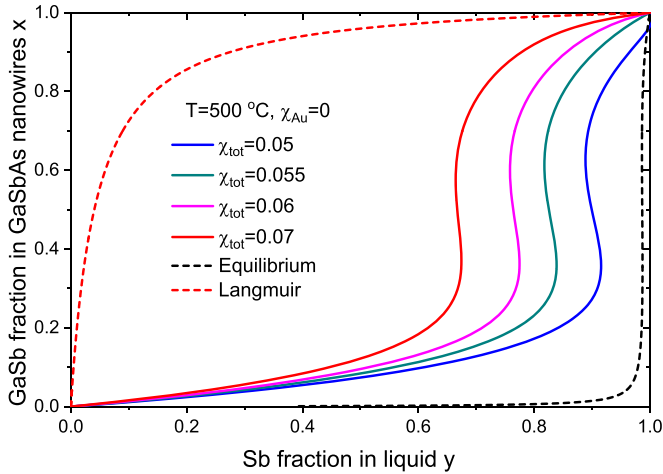


FIG. 7. Same as Fig. 6 for self-catalyzed $\text{Ga}_{1-x}\text{Sb}_x\text{As}_{1-x}$ NWs at 500 °C. Below $\chi_{\text{tot}} \cong 0.05$, Ga droplets are undersaturated and no VLS growth is possible.

at low χ_{tot} , is suppressed by the liquid-solid growth kinetics at high χ_{tot} .

Figure 7 shows the kinetic liquid-solid distributions of self-catalyzed $\text{GaSb}_x\text{As}_{1-x}$ NWs at 500 °C, with $\omega = 2.184$, $\omega_{\text{GaSb}} = -1.32$, $\omega_{\text{GaAs}} = -4.49$, $\Delta\mu_{\text{GaSb}}^0 = 4.33$, and $\Delta\mu_{\text{GaAs}}^0 = 11.79$, according to Refs. [57,59], assuming $D_{\text{Sb}}/D_{\text{As}} = 1$. Due to a low value of $\Delta\mu_{\text{GaSb}}^0$, the self-catalyzed VLS growth of GaSbAs NWs requires high total concentrations of group V atoms in Ga droplet ($\chi_{\text{tot}} > 0.05$). The droplet remains undersaturated at $\chi_{\text{tot}} < 0.05$, which corresponds to the no-growth conditions. Such high concentrations are hardly accessible for As, but may be reached due to a higher solubility of Sb in liquid Ga and generally in Au-group III liquid melts [37]. The liquid-solid distributions are far from the purely kinetic Langmuir-McLean curve for a plausible range of χ_{tot} from 0.05 to 0.07, and the miscibility gap is not circumvented.

To conclude this section, the liquid-solid distributions of VLS ternary NWs based on group V intermix are kinetically controlled because the liquid-solid growth is limited by the attachment of group V atoms in the excess of group III atoms. Equation (28) or simplified Eq. (29), which have the same form as the earlier results obtained within the binary growth model [47–50] and the kinetic vapor-solid distribution of Ref. [52], should work well for all group V-based ternary NWs. Importantly, the miscibility gaps and the nonlinearity of the equilibrium distribution shapes can be fully circumvented at high enough group V concentrations, leading to the purely kinetic Langmuir-McLean distribution. The nucleation-limited model [42–44] or the equilibrium model [41], yielding the same liquid-solid distribution [41,41], should not be used for group V intermixes. For VLS ternary NWs based on group III intermix, the situation is reversed. Their liquid-solid growth typically occurs under group III-rich conditions in the catalyst droplets, which renders the liquid-solid distribution into the nucleation-limited or close-to-equilibrium regime [41–44]. Equation (34) or its approximation given by Eq. (35) accounts for the kinetic corrections and allows one to describe the experimen-

tally observed kinetic suppression of the miscibility gap in Au-catalyzed InGaAs NWs [19]. However, these equations describe close-to-equilibrium nonlinear distribution shapes due to large $\varepsilon \gg 1$. The kinetic models of Refs. [47–50] and their generalizations [40] should not be used for VLS NWs based on group III intermix, because their vapor-liquid growth is not limited by the attachment of group III atoms.

IV. VAPOR-SOLID DISTRIBUTIONS

Most experimental works [14–18,20,22–25,29–36], with only one exception [19], reported the measured vapor-solid distributions of VLS III-V ternary NWs, while the liquid-solid distributions were used mainly for modeling the interfacial abruptness across axial NW heterostructures [21,28,38,43,50]. A more practically relevant vapor-solid distribution presents the NW composition x as a function of the technologically controlled A content in vapor, $z = I_A/(I_A + I_B)$, rather than the fraction of A atoms in liquid $y = \chi_A/(\chi_A + \chi_B)$, which is principally unknown for VLS NWs based on group V intermix and beyond control for VLS NWs based on group III intermix in most cases. Linking the liquid composition given by the three atomic concentrations χ_A , χ_B , and χ_C to the vapor fluxes I_A , I_B , and I_C is not a simple problem for the following reason. In the kinetic approach developed in the previous section, the liquid-solid distribution was determined in the stage of monolayer growth assuming time-independent χ_A , χ_B , and χ_C , as in Refs. [47–50]. However, the axial NW growth rate is not determined by the monolayer growth rate but rather by the waiting time between the successive nucleation events [13,60]. The situation becomes even more complex at low concentrations of group V atoms in small enough catalyst droplets. Insufficient amount of group V atoms present in the droplet before nucleation and slow refill from vapor (compared to the monolayer growth) may lead to dropping the liquid-solid supersaturation level to zero before the monolayer completion. In this case, the fast-growth stage stops at a certain monolayer size. After that, the monolayer is completed either at a slow rate of refill (for wurtzite III-V NWs with the planar growth interface) or by rapidly transferring III-V pairs from the truncation (for zincblende III-V NWs with the truncated growth interface) [61–64]. These effects may significantly influence the NW composition and require a separate theoretical treatment which will be presented elsewhere.

In this work, we use the simple material balance equations for the vapor-solid growth of a ternary NW in the form [13,45,52]

$$\frac{\pi R^2}{\Omega_s} x \frac{dL}{dt} = V_A^+ - V_A^-, \quad \frac{\pi R^2}{\Omega_s} (1-x) \frac{dL}{dt} = V_B^+ - V_B^-. \quad (36)$$

Here, R is the radius of the NW top, Ω_s is the elementary volume per III-V pair in solid, V_A^+ , V_B^+ are the total numbers of A and B atoms arriving to the droplet per unit time by different kinetic pathways, and V_A^- , V_B^- are the corresponding numbers of atoms leaving the droplet, or the effective desorption rates. Regardless of the form of the NW axial growth rate dL/dt ,

Eq. (36) results in

$$\frac{1-x}{x} = \frac{V_B^+ - V_B^-}{V_A^+ - V_A^-}. \quad (37)$$

The effective desorption rates V_A^- and V_B^- are independent of the vapor fluxes and can be related to the liquid composition using the above model for the liquid-solid distribution.

We first consider VLS ternary NWs based on group III intermix. The arrival rates of A and B atoms into the droplet are proportional to the vapor fluxes [22,40,45,52]:

$$\begin{aligned} V_A^+ &= (\sigma_A \pi R^2 + \eta_A 2\pi R \lambda_A) I_A, \\ V_B^+ &= (\sigma_B \pi R^2 + \eta_B 2\pi R \lambda_B) I_B. \end{aligned} \quad (38)$$

These rates contain the R^2 direct-impingement terms, with σ_k as the precursor decomposition efficiencies in MOVPE or geometrical coefficients in molecular-beam epitaxy (MBE). The R terms describe surface diffusion of A and B adatoms from the NW sidewalls to the droplet, with η_k as the precursor decomposition efficiencies at the NW sidewalls in MOVPE or geometrical coefficients in MBE, and λ_k as the effective diffusion lengths of adatoms on the NW sidewalls. Diffusion from the substrate surface may also be included using the radius and pitch-dependent λ_k [13,40,52]. For III-V NW growth, group III atoms usually leave the droplet by “negative” diffusion from the droplet onto the NW sidewalls rather than by the direct desorption from the droplet surface, at least in MBE technique [13,45,65,66]. These adatoms subsequently evaporate or incorporate into the vapor-solid shells growing around the VLS NW core, in which case the diffusion lengths λ_k are incorporation limited.

In order to find the negative-diffusion fluxes, we use the diffusion equations for the surface concentrations n_k of A and B adatoms on the NW sidewalls [52]:

$$D_{k,a} \frac{d^2 n_k}{d\xi^2} + \eta_k I_k - \frac{n_k}{\tau_k} = 0, \quad k = A, B, \quad (39)$$

with ξ as the vertical coordinate, $D_{k,a}$ as the surface diffusion coefficients, τ_k as the effective lifetimes. The boundary conditions far away from the droplet are taken in the form

$$n_k(\xi \rightarrow \infty) = \eta_k \tau_k I_k, \quad k = A, B. \quad (40)$$

For the adsorbing boundary conditions at the triple-phase line under the droplet, we use the chemical potentials of noninteracting A and B adatoms in the form $\mu_k^a = \mu_k^0 + \ln \theta_k$, where $\theta_k = \Omega_l^{2/3} n_k$ are the adatom coverages [52,53]. These chemical potentials must equal the chemical potentials of A and B atoms in the droplet: $\mu_k^a(\xi = 0) = \mu_k$, which yields

$$n_k(\xi = 0) = n_{k*} = \frac{1}{\Omega_l^{2/3}} e^{\mu_k - \mu_k^0}, \quad k = A, B. \quad (41)$$

The total diffusion fluxes into the droplet are easily obtained in the form

$$\begin{aligned} V_{k,\text{diff}} &= 2\pi R D_{k,a} \left. \frac{dn_k}{d\xi} \right|_{\xi=0} = 2\pi R \lambda_k \left(\eta_k I_k - \frac{n_{k*}}{\tau_k} \right), \\ k &= A, B. \end{aligned} \quad (42)$$

Using Eq. (5), the negative-diffusion fluxes are proportional to the atomic concentrations of A and B atoms in the

droplet:

$$V_A^- = 2\pi R \frac{\lambda_A}{\tau_A} \frac{1}{\Omega_l^{2/3}} e^{\psi_A} \chi_A, \quad V_B^- = 2\pi R \frac{\lambda_B}{\tau_B} \frac{1}{\Omega_l^{2/3}} e^{\psi_B} \chi_B. \quad (43)$$

Together with Eq. (37) and with the known liquid-solid distribution $x(y)$, this allows one to link the solid composition to the vapor composition.

The vapor-solid equilibrium in a ternary VLS system corresponds to $V_A^+ = V_A^-$ and $V_B^+ = V_B^-$, where no VLS growth occurs. Using Eqs. (38) and (43), the equilibrium vapor-solid distribution is given by

$$z = \frac{y}{c_g/\gamma + (1 - c_g/\gamma)y}, \quad (44)$$

with

$$c_g = \frac{\sigma_A + 2\eta_A \lambda_A/R}{\sigma_B + 2\eta_B \lambda_B/R}, \quad \gamma = \frac{\lambda_A \tau_B}{\lambda_B \tau_A} e^{\psi_A - \psi_B}. \quad (45)$$

The coefficient c_g accounts for the different arrival rates of A and B atoms and is independent of the liquid state, while γ accounts for the different rates of A and B atoms leaving the droplet and may depend on the liquid composition through the $\exp(\psi_A - \psi_B)$ factor. For the equilibrium liquid-solid distribution $y = 1/[1 + f(x)]$, with $f(x)$ given by Eq. (23), the vapor-solid equilibrium distribution is reduced to

$$\begin{aligned} z &= \frac{1}{1 + F(x)}, \\ F(x) &= \left(\frac{\sigma_A + 2\eta_A \lambda_A/R}{\sigma_B + 2\eta_B \lambda_B/R} \right) \frac{\lambda_B}{\lambda_A} \beta_g \frac{(1-x)}{x} e^{\omega(2x-1)} \\ &\rightarrow \beta_g \frac{(1-x)}{x} e^{\omega(2x-1)}. \\ \beta_g &= \frac{\tau_A}{\tau_B} e^{\Delta\mu_{AC}^0 - \Delta\mu_{BC}^0}. \end{aligned} \quad (46)$$

At $2\eta_k \lambda_k/R \gg \sigma_k$ for both A and B atoms, this equilibrium distribution is equivalent to the result of Ref. [52], which was obtained for the vapor-solid growth without any droplet. Importantly, the obtained result contains no characteristics of liquid, showing that the equilibrium vapor-solid distribution of VLS NWs is independent of the droplet composition, the presence or absence of Au, and the unknown group V concentration.

In the general case, the vapor-solid distribution is obtained from Eqs. (37), (38), and (43) in the form

$$z = \frac{x + \alpha[\gamma(1-x)y(x) - x(1-y(x))]}{c_g + (1 - c_g)x}, \quad (47)$$

with

$$\alpha = \frac{1}{(\sigma_B R/2\lambda_B + \eta_B)} \frac{1}{\tau_B} \frac{\chi_{\text{tot}}}{\Omega_l^{2/3} I_{\text{tot}}} e^{\psi_B}. \quad (48)$$

Clearly, the parameter α describes the influence of “desorption” processes, and is related to the vapor supersaturation with respect to liquid (which may depend on the total V/III flux ratio). At $\alpha \rightarrow 0$, the vapor-solid distribution is reduced

to the kinetic Langmuir-McLean formula:

$$z = \frac{x}{c_g + (1 - c_g)x}, \quad (49)$$

which contains no characteristics of liquid, as in Refs. [22,25,45,52]. For the $y(x)$ dependence in the general equation (47), one can use the equilibrium liquid-solid distribution given by Eq. (30) according to the results of the previous section.

For VLS NWs based on group V intermix, group V atoms arrive at the droplet directly from vapor [13], and usually desorb in the form of V_2 dimers [13,46,63,64]. Therefore, we can use

$$V_A^+ = \sigma_A \pi R^2 I_A, \quad V_B^+ = \sigma_B \pi R^2 I_B. \quad (50)$$

$$V_A^- = \frac{D_A e^{\psi_A}}{\Omega_l^{4/3}} \frac{2\pi R^2}{(1 + \cos\beta)} 2\chi_A^2, \quad (51)$$

$$V_B^- = \frac{D_B e^{\psi_B}}{\Omega_l^{4/3}} \frac{2\pi R^2}{(1 + \cos\beta)} 2\chi_B^2.$$

Here, σ_k are the precursor decomposition efficiencies in MOVPE or geometrical coefficients in MBE. The desorption fluxes V_k^- are assumed proportional to the diffusion fluxes $d_k \alpha_k$ times the surface concentration $\chi_k / \Omega_l^{2/3}$, which results in the quadratic dependence of the desorption rates on χ_k [46,63,64]. The equilibrium vapor-solid distribution, corresponding to $V_A^+ = V_A^-$, $V_B^+ = V_B^-$, is given by

$$z = \frac{y^2}{y^2 + (c_g/c_l)(1 - y)^2}, \quad (52)$$

with

$$c_g = \frac{\sigma_A}{\sigma_B} \quad (53)$$

and c_l given by Eq. (29). In the general case, the vapor-solid distribution of VLS NWs based on group V intermix has the form

$$z = \frac{x + \alpha[\gamma(1 - x)y^2(x) - x(1 - y^2(x))]}{c_g + (1 - c_g)x}. \quad (54)$$

Here, one can use the kinetic $y(x)$ dependence given by Eq. (28) or Eq. (29) according to the results of the previous section. The parameter

$$\alpha = \frac{4}{\sigma_B(1 + \cos\beta)} \frac{D_B e^{\psi_B}}{\Omega_l^{2/3}} \frac{\chi_{\text{tot}}^2}{\Omega_l^{2/3} I_{\text{tot}}} \quad (55)$$

describing the desorption processes, contains the unknown total concentration of group V atoms χ_{tot} . Therefore, the uncertainty in the liquid composition is not fully circumvented in the model given by Eq. (37), which is why the vapor-solid distribution of VLS NWs based on group V intermix requires further studies. At $\alpha \rightarrow 0$, corresponding to a rare case of negligible desorption of group V atoms from a catalyst droplet, the vapor-solid distribution is reduced to the purely kinetic Langmuir-McLean expression given by Eq. (49). The coefficient $c_g = \sigma_A/\sigma_B$ describes the vapor-solid incorporation ratio of A over B atoms. Such a dependence was reported for self-catalyzed GaAsP NWs grown on silicon by MBE [30].

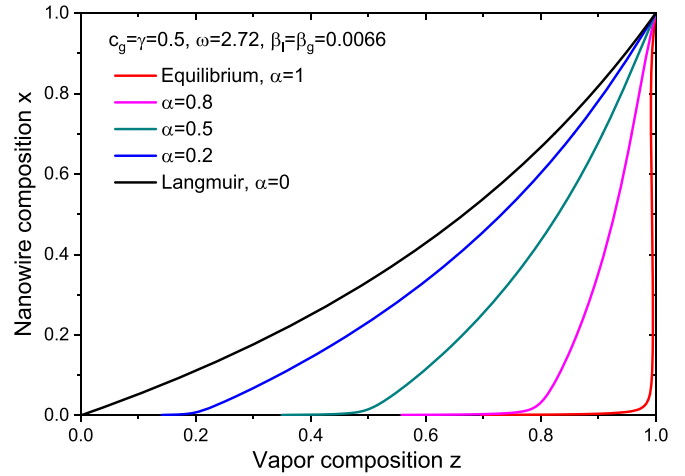


FIG. 8. Vapor-solid distributions of VLS NWs based on group III intermix, obtained from Eq. (47) at different α shown in legend. Distribution changes from the equilibrium shape at $\alpha = 1$, containing miscibility gap, to purely kinetic Langmuir-McLean shape at $\alpha = 0$.

Figure 8 shows the vapor-solid distributions of VLS NWs based on group III intermix, obtained from Eq. (47) at a fixed $c_g = \gamma = 0.5$, $\omega = 2.72$, and $\beta_l = \beta_g = 0.0066$ (the last two parameters approximately correspond to $\text{In}_x\text{Ga}_{1-x}\text{As}$ NWs at 380°C). With these parameters, the equilibrium state corresponding to zero fluxes is reached at $\alpha = 1$. Decreasing the α parameter from 1 to 0 gradually transforms the vapor-solid distribution from the nonlinear equilibrium shape with the miscibility gap to the purely kinetic regime, where the miscibility gap is fully circumvented and the $x(z)$ dependence is governed by the sole kinetic parameter c_g .

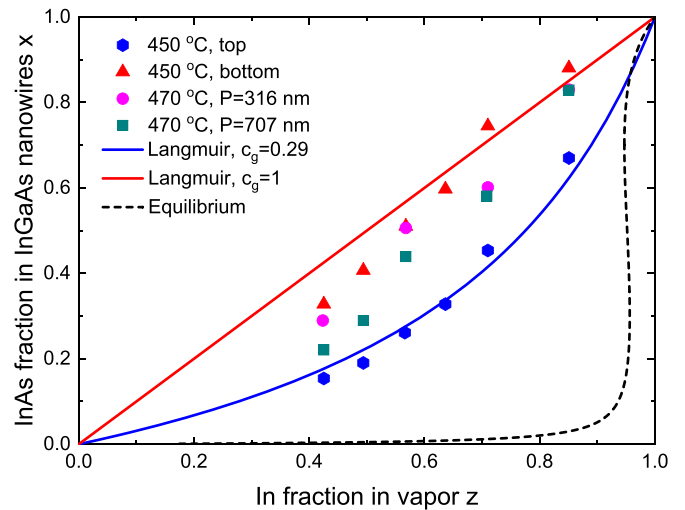


FIG. 9. Vapor-solid distributions of Au-catalyzed InGaAs NWs grown by MOVPE at 450°C and 470°C and two different average distances between NWs P , with NW compositions measured at NW tops and bottoms [16] (symbols). All data points are restricted by two purely kinetic Langmuir-McLean curves with $c_g = 0.29$ and 1 (solid lines), and very far from equilibrium distribution shown by dashed line.

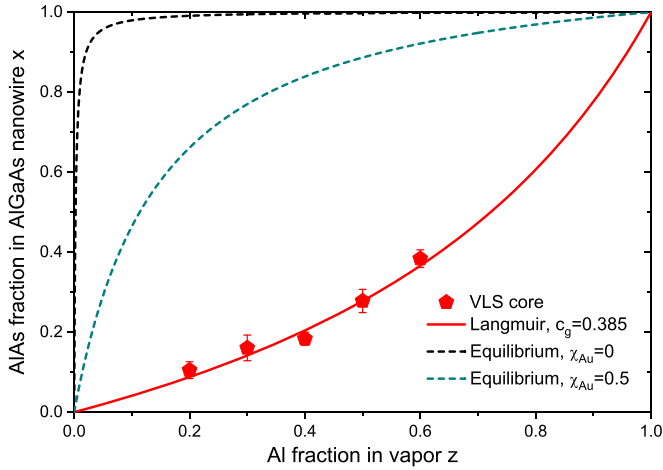


FIG. 10. Vapor-solid distribution in VLS cores of Au-catalyzed AlGaAs NWs grown by MBE at 510 °C [22] (symbols), fitted by Langmuir-McLean kinetic curve at $c_g = 0.385$ (solid line). Data points are far from nonlinear liquid-solid distributions of VLS AlGaAs NWs shown by dashed lines for self-catalyzed ($\chi_{\text{Au}} = 0$) and Au-catalyzed ($\chi_{\text{Au}} = 0.5$) NWs.

Figure 9 shows the vapor-solid distributions of Au-catalyzed $\text{In}_x\text{Ga}_{1-x}\text{As}$ NWs, grown by MOVPE on InAs(111)B substrates using 50-nm-diameter Au nanoparticles. Different vapor compositions were achieved by varying fluxes of In and Ga precursors. For 3000-nm-long NWs grown at 450 °C with a V/III flux ratio of 12.6, the composition was measured at the NW top and bottom. The average distance P between these NWs was 707 nm. At a temperature of 470 °C and a V/III flux ratio of 6.32, 1200-nm-long InGaAs NWs were grown with two different surface densities of Au nanoparticles corresponding to P of 316 and 707 nm. For these NWs, the composition was measured at the NW tops. All these data points are restricted by the two purely kinetic Langmuir-McLean curves given by Eq. (49) at $c_g = 0.29$ and 1, corresponding to different mechanisms of the diffusion transport of In and Ga adatoms into the droplets for short and long NWs. The equilibrium vapor-solid distribution at 450 °C, shown by the dashed line in the figure, is similar to the equilibrium liquid-solid distributions in Figs. 3, and 4. It is seen that the data points are very far from equilibrium. Therefore, the observed vapor-solid compositional trends are driven by the kinetic factors rather than by thermodynamics, and independent of the liquid state, as in Fig. 8 at $\alpha \rightarrow 0$.

Figure 10 shows the vapor-solid distribution in the cores of Au-catalyzed VLS $\text{Al}_x\text{Ga}_{1-x}\text{As}$ nanowires of Ref. [20], grown by MBE on Si(111) substrates at 510 °C. The Au droplets were obtained by thermal dewetting of thin Au films deposited onto the substrates. Different vapor compositions were achieved by varying the Al and Ga fluxes at a fixed total group III flux, with a V/III flux ratio of 3. Spontaneous formation of the core-shell AlGaAs structures was observed, with higher AlAs fractions in the shells. Cylindrical cores were formed by the VLS mechanism, while conical shells were grown in the vapor-solid mode around the VLS shells. The AlAs fractions in the shells were very close to the Al fractions in vapor [20]. The AlAs fractions in the VLS cores were systematically

lower than the Al fractions in vapor, which was attributed to a lower Al diffusivity on the NW sidewalls compared to Ga. The vapor-solid distribution in the VLS cores is well fitted by the kinetic Langmuir-McLean formula with $c_g = 0.385$ [20,52]. As in the previous case, this distribution is very far from the equilibrium liquid-solid distributions of VLS AlGaAs NWs, which have no miscibility gap due to $\omega \cong 0$ but require low fractions of Al atoms in liquid [21,43,44], particularly in the self-catalyzed VLS growth [21].

As a general conclusion of this section, the vapor-solid distributions of VLS III-V ternary NWs can be modeled using the simplified approach based on Eq. (37). In this model, the desorption rates of A and B atoms from the droplet depend on the known liquid-solid distribution $y(x)$, while the arrival rates depend on z , which allows one to relate the solid and vapor compositions. At low enough desorption rates from the droplet, which is relevant for group III atoms in many cases, the vapor-solid distributions of VLS NWs are simply given by the kinetic Langmuir-McLean formula and independent of the liquid composition.

V. CONCLUSIONS

In summary, our model for the stationary compositions of VLS III-V ternary NWs presents the liquid-solid distribution in the form of a combination of the equilibrium (or nucleation-limited) and kinetic distributions. Both equilibrium [41–44] and kinetic [47] liquid-solid distributions were considered previously, however, without clear differentiation of the relevant ternary NWs to which they apply. The developed approach shows that the close-to-equilibrium shape applies to VLS NWs based on group III intermix, whose liquid-solid growth occurs under group III-rich conditions. The kinetic models should not be used for such NWs. Conversely, the kinetically controlled liquid-solid distribution applies to VLS NWs based on group V intermix, whose liquid-solid growth occurs under group V-poor conditions. The equilibrium liquid-solid distributions should not be used for such NWs. The vapor-solid distributions of VLS III-V ternary NWs were studied within a simplified approach that ignores many important factors, including the droplet depletion with its group V atoms during the monolayer growth [62–64], and the influence of the total V/III flux ratio on the axial NW growth rate [13] and the liquid composition. We plan to study these factors in detail in a separate paper. However, this model reveals the experimentally observed trend for kinetically controlled vapor-solid distribution shapes of III-V NWs based on group III intermix [16–18,25]. This can be understood using the vapor-solid growth model without any droplet [52]. The obtained results for the liquid-solid distributions of different III-V NWs can be used in modeling of the nonstationary growth process of forming III-V NW heterostructures and their interfacial abruptness [21,43,50], and applied to other pseudobinary material systems.

ACKNOWLEDGMENT

The author gratefully acknowledges financial support from the research grant of St. Petersburg State University (Grant No. ID 94033852).

- [1] M. B. Panish and M. Ilegams, *Progress in Solid State Chemistry* (Pergamon Press, New York, 1972), Vol. 7.
- [2] R. M. Biefeld, The preparation of InSb and InAs_{1-x}Sb_x by metalorganic chemical vapor deposition, *J. Cryst. Growth* **75**, 255 (1986).
- [3] C.-Z. Ning, L. Dou, and P. Yang, Bandgap engineering in semiconductor alloy nanomaterials with widely tunable compositions, *Nat. Rev. Mater.* **2**, 17070 (2017).
- [4] P. C. McIntyre and A. Fontcuberta i Morral, Semiconductor nanowires: To grow or not to grow? *Mater. Today Nano* **9**, 100058 (2020).
- [5] J. K. Hyun, S. Zhang, and L. J. Lauhon, Nanowire heterostructures, *Annu. Rev. Mater. Res.* **43**, 451 (2013).
- [6] G. Boras, X. Yu, and H. Liu, III-V ternary nanowires on Si substrates: growth, characterization and device applications, *J. Semicond.* **40**, 101301 (2019).
- [7] F. Martelli, III-V ternary nanowires, in *Advances in III-V Semiconductor Nanowires and Nanodevices*, edited by J. Li, D. Wang, and R. R. LaPierre (2011), pp. 105–128.
- [8] F. Glas, Critical dimensions for the plastic relaxation of strained axial heterostructures in free-standing nanowires, *Phys. Rev. B* **74**, 121302(R) (2006).
- [9] L. C. Chuang, M. Moewe, C. Chase, N. P. Kobayashi, C. Chang-Hasnain, and S. Crankshaw, Critical diameters for III-V nanowires grown on lattice-mismatched substrates, *Appl. Phys. Lett.* **90**, 043115 (2007).
- [10] V. G. Dubrovskii, N. V. Sibirev, X. Zhang, and R. A. Suris, Stress-driven nucleation of three-dimensional crystal islands: From quantum dots to nanoneedles, *Cryst. Growth Des.* **10**, 3949 (2010).
- [11] R. S. Wagner and W. C. Ellis, Vapor-liquid-solid mechanism of single crystal growth, *Appl. Phys. Lett.* **4**, 89 (1964).
- [12] C. Colombo, D. Spirkoska, M. Frimmer, G. Abstreiter, and A. Fontcuberta i Morral, Ga-assisted catalyst-free growth mechanism of GaAs nanowires by molecular beam epitaxy, *Phys. Rev. B* **77**, 155326 (2008).
- [13] V. G. Dubrovskii and F. Glas, Vapor-liquid-solid growth of semiconductor nanowires, in *Fundamental Properties of Semiconductor Nanowires*, edited by N. Fukata and R. Rurali (Springer, Singapore, 2020).
- [14] I. Regolin, V. Khorenko, W. Prost, F.-J. Tegude, D. Sudfeld, J. Kästner, and G. Dumpich, Composition control in metalorganic vapor-phase epitaxy grown InGaAs nanowhiskers, *J. Appl. Phys.* **100**, 074321 (2006).
- [15] C. S. Jung, H. S. Kim, G. B. Jung, K. J. Gong, Y. J. Cho, S. Y. Jang, C. H. Kim, C.-W. Lee, and J. Park, Composition and phase tuned InGaAs alloy nanowires, *J. Phys. Chem. C* **115**, 7843 (2011).
- [16] J. Wu, M. Borg, D. Jacobsson, K. A. Dick, and L. E. Wernersson, Control of composition and morphology in InGaAs nanowires grown by metalorganic vapor phase epitaxy, *J. Cryst. Growth* **383**, 158 (2013).
- [17] A. S. Ameruddin, H. A. Fonseka, P. Caroff, J. Wong-Leung, R. L. M. O. Veld, J. L. Boland, M. B. Johnston, H. H. Tan, and C. Jagadish, In_xGa_{1-x}As nanowires with uniform composition, pure wurtzite crystal phase and taper-free morphology, *Nanotechnology* **26**, 205604 (2015).
- [18] A. S. Ameruddin, P. Caroff, H. H. Tan, C. Jagadish, and V. G. Dubrovskii, Understanding the growth and composition evolution of gold-seeded ternary InGaAs nanowires, *Nanoscale* **7**, 16266 (2015).
- [19] R. Sjökvist, D. Jacobsson, M. Tornberg, R. Wallenberg, E. D. Leshchenko, J. Johansson, and K. A. Dick, Compositional correlation between the nanoparticle and the growing Au-assisted In_xGa_{1-x}As nanowire, *J. Phys. Chem. Lett.* **12**, 7590 (2021).
- [20] D. Jacobsson, J. M. Persson, D. Kriegner, T. Etzelstorfer, J. Wallentin, J. B. Wagner, J. Stangl, L. Samuelson, K. Deppert, and M. T. Borgstrom, Particle-assisted Ga_xIn_{1-x}P nanowire growth for designed bandgap structures, *Nanotechnology* **23**, 245601 (2012).
- [21] G. Priante, F. Glas, G. Patriarche, K. Pantzas, F. Oehler, and J. C. Harmand, Sharpening the interfaces of axial heterostructures in self-catalyzed AlGaAs nanowires: Experiment and theory, *Nano Lett.* **16**, 1917 (2016).
- [22] V. G. Dubrovskii, I. V. Shtrom, R. R. Reznik, Yu. B. Samsonenko, A. I. Khrebtov, I. P. Soshnikov, S. Rouvimov, N. Akopian, T. Kasama, and G. E. Cirlin, Origin of spontaneous core-shell AlGaAs nanowires grown by molecular beam epitaxy, *Cryst. Growth Des.* **16**, 7251 (2016).
- [23] C. Chen, S. Shehata, C. Fradin, R. R. LaPierre, C. Couteau, and G. Weihs, Self-directed growth of AlGaAs core-shell nanowires for visible light applications, *Nano Lett.* **7**, 2584 (2007).
- [24] S. G. Ghalamestani, M. Ek, B. Ganjipour, C. Thelander, J. Johansson, P. Caroff, and K. A. Dick, Demonstration of defect-free and composition tunable Ga_xIn_{1-x}Sb_x nanowires, *Nano Lett.* **12**, 4914 (2012).
- [25] E. Roche, Y. André, G. Avit, C. Bougerol, D. Castelluci, F. Réveret, E. Gil, F. Médard, J. Leymarie, T. Jean, V. G. Dubrovskii, and A. Trassoudain, Circumventing the miscibility gap in InGaN nanowires emitting from blue to red, *Nanotechnology* **29**, 465602 (2018).
- [26] A. I. Persson, M. T. Björk, S. Jeppesen, J. B. Wagner, L. R. Wallenberg, and L. Samuelson, InAs_{1-x}P_x nanowires for device engineering, *Nano Lett.* **6**, 403 (2006).
- [27] B. Mandl, M. Keplinger, M. E. Messing, D. Kriegner, R. Wallenberg, L. Samuelson, G. Bauer, J. Stangl, V. Holý, and K. Deppert, Self-seeded axio-radial InAs – InAs_{1-x}P_x nanowire heterostructures beyond “common” VLS growth, *Nano Lett.* **18**, 144 (2018).
- [28] V. Zannier, F. Rossi, V. G. Dubrovskii, D. Ercolani, S. Battiato, and L. Sorba, Nanoparticle stability in axial InAs–InP nanowire heterostructures with atomically sharp interfaces, *Nano Lett.* **18**, 167 (2018).
- [29] Y. Zhang, A. M. Sanchez, Y. Sun, J. Wu, M. Aagesen, S. Huo, D. Kim, P. Jurczak, X. Xu, and H. Liu, Influence of droplet size on the growth of self-catalyzed ternary GaAsP nanowires, *Nano Lett.* **16**, 1237 (2016).
- [30] Y. Zhang, M. Aagesen, J. V. Holm, H. I. Jørgensen, J. Wu, and H. Liu, Self-catalyzed GaAsP nanowires grown on silicon substrates by solid-source molecular beam epitaxy, *Nano Lett.* **13**, 3897 (2013).
- [31] B. M. Borg, K. A. Dick, J. Eymery, and L.-E. Wernersson, Enhanced Sb incorporation in InAsSb nanowires grown by metalorganic vapor phase epitaxy, *Appl. Phys. Lett.* **98**, 113104 (2011).
- [32] L. Namazi, S. G. Ghalamestani, S. Lehmann, R. R. Zamani, and K. A. Dick, Direct nucleation, morphology and compositional tuning of InAs_{1-x}Sb_x nanowires on InAs (111)B substrates, *Nanotechnology* **28**, 165601 (2017).

- [33] Q. D. Zhuang, H. Alradhi, Z. M. Jin, X. R. Chen, J. Shao, X. Chen, A. M. Sanchez, Y. C. Cao, J. Y. Liu, P. Yates, K. Durose, and C. J. Jin, Optically-efficient InAsSb nanowires for silicon-based mid-wavelength infrared optoelectronics, *Nanotechnology* **28**, 105710 (2017).
- [34] X. Yuan, P. Caroff, J. Wong-Leung, H. H. Tan, and C. Jagadish, Controlling the morphology, composition and crystal structure in gold-seeded GaAs_{1-x}Sb_x nanowires, *Nanoscale* **7**, 4995 (2015).
- [35] L. Li, D. Pan, Y. Xue, X. Wang, M. Lin, D. Su, Q. Zhang, X. Yu, H. So, D. Wei, B. Sun, P. Tan, A. Pan, and J. Zhao, Near full-composition-range high-quality GaAs_{1-x}Sb_x nanowires grown by molecular-beam epitaxy, *Nano Lett.* **17**, 622 (2017).
- [36] S. Conesa-Boj, D. Kriegner, X.-L. Han, S. Plissard, X. Wallart, J. Stangl, A. Fontcuberta i Morral, and P. Caroff, Gold-free ternary III-V antimonide nanowire arrays on silicon: Twin-free down to the first bilayer, *Nano Lett.* **14**, 326 (2014).
- [37] L. Lugani, D. Ercolani, L. Sorba, N. V. Sibirev, M. A. Timofeeva, and V. G. Dubrovskii, Modeling of InAs-InSb nanowires grown by Au-assisted chemical beam epitaxy, *Nanotechnology* **23**, 095602 (2012).
- [38] V. G. Dubrovskii, Understanding the vapor-liquid-solid growth and composition of ternary III-V nanowires and nanowire heterostructures, *J. Phys. D: Appl. Phys.* **50**, 453001 (2017).
- [39] M. Ghasemi, E. D. Leshchenko, and J. Johansson, Assembling your nanowire: An overview of composition tuning in ternary III-V nanowires, *Nanotechnology* **32**, 072001 (2021).
- [40] E. D. Leshchenko and V. G. Dubrovskii, An overview of modeling approaches for compositional control in III-V ternary nanowires, *Nanomaterials* **13**, 1659 (2023).
- [41] F. Glas, Comparison of modeling strategies for the growth of heterostructures in III-V nanowires, *Cryst. Growth Des.* **17**, 4785 (2017).
- [42] J. Johansson and M. Ghasemi, Composition of gold alloy seeded InGaAs nanowires in the nucleation limited regime, *Cryst. Growth Des.* **17**, 1630 (2017).
- [43] V. G. Dubrovskii, A. A. Koryakin, and N. V. Sibirev, Understanding the composition of ternary III-V nanowires and axial nanowire heterostructures in nucleation-limited regime, *Mater. Design* **132**, 400 (2017).
- [44] E. D. Leshchenko, M. Ghasemi, V. G. Dubrovskii, and J. Johansson, Nucleation-limited composition of ternary III-V nanowires forming from quaternary gold based liquid alloys, *CrystEngComm* **20**, 1649 (2018).
- [45] V. G. Dubrovskii, Fully analytical description for the composition of ternary vapor-liquid-solid nanowires, *Cryst. Growth Des.* **15**, 5738 (2015).
- [46] V. G. Dubrovskii, Compositional control of gold-catalyzed ternary nanowires and axial nanowire heterostructures based on III-P_{1-x}As_x, *J. Cryst. Growth* **498**, 179 (2018).
- [47] J. Johansson and M. Ghasemi, Kinetically limited composition of ternary III-V nanowires, *Phys. Rev. Mater.* **1**, 040401(R) (2017).
- [48] E. D. Leshchenko and J. Johansson, Role of thermodynamics and kinetics in the composition of ternary III-V nanowires, *Nanomaterials* **10**, 2553 (2020).
- [49] E. K. Mårtensson, J. Johansson, and K. A. Dick, Simulating vapor-liquid-solid growth of Au-seeded InGaAs nanowires, *ACS Nanosci. Au* **2**, 239 (2022).
- [50] E. D. Leshchenko and V. G. Dubrovskii, Kinetic modeling of interfacial abruptness in axial nanowire heterostructures, *Nanotechnology* **34**, 065602 (2023).
- [51] D. McLean, *Grain Boundaries in Metals* (Oxford University Press, New York, 1957).
- [52] V. G. Dubrovskii and E. D. Leshchenko, Kinetically controlled composition of III-V ternary nanostructures, *Phys. Rev. Mater.* **7**, 056001 (2023).
- [53] V. G. Dubrovskii and E. D. Leshchenko, Composition of III-V ternary materials under arbitrary material fluxes: The general approach unifying kinetics and thermodynamics, *Phys. Rev. Mater.* **7**, 074603 (2023).
- [54] J. Keizer, *Statistical Thermodynamics of Nonequilibrium Processes* (Springer, Berlin, 1987).
- [55] V. G. Dubrovskii, Fluctuation-induced spreading of size distribution in condensation kinetics, *J. Chem. Phys.* **131**, 164514 (2009).
- [56] V. G. Dubrovskii and J. Greckov, Zeldovich nucleation rate, self-consistency renormalization, and crystal phase of Au-catalyzed GaAs nanowires, *Cryst. Growth Des.* **15**, 340 (2015).
- [57] I. Ansara, C. Chatillon, H. L. Lukas, T. Nishizawa, H. Ohtani, K. Ishida, M. Hillert, B. Sundman, B. B. Argent, A. Watson *et al.*, A binary database for III-V compound semiconductor systems, *Calphad* **18**, 177 (1994).
- [58] W.-K. Chen and M.-T. Chin, Influence of thermodynamic factors on growth of AlAs_{1-x}Sb_x Alloys, *Jpn. J. Appl. Phys.* **33**, L1370 (1994).
- [59] J.-M. Lin, L.-C. Chou, and H.-H. Lin, Combination of thermodynamic model and precursor state for As and Sb incorporation behavior in GaAsSb/GaAs multiple-quantum wells, *J. Vac. Sci. Technol.*, **B 29**, 021011 (2011).
- [60] V. G. Dubrovskii, N. V. Sibirev, J. C. Harmand, and F. Glas, Growth kinetics and crystal structure of semiconductor nanowires, *Phys. Rev. B* **78**, 235301 (2008).
- [61] V. G. Dubrovskii, Refinement of nucleation theory for vapor-liquid-solid nanowires, *Cryst. Growth Des.* **17**, 2589 (2017).
- [62] J. C. Harmand, G. Patriarche, F. Glas, F. Panciera, I. Florea, J. L. Maurice, L. Travers, and Y. Ollivier, Atomic Step Flow on a Nanofacet, *Phys. Rev. Lett.* **121**, 166101 (2018).
- [63] F. Glas and V. G. Dubrovskii, Energetics and kinetics of monolayer formation in vapor-liquid-solid nanowire growth, *Phys. Rev. Mater.* **4**, 083401 (2020).
- [64] F. Glas, F. Panciera, and J. C. Harmand, Statistics of nucleation and growth of single monolayers in nanowires: Towards a deterministic regime, *Phys. Stat. Solidi RRL* **16**, 2100647 (2022).
- [65] M. C. Plante and R. R. LaPierre, Analytical description of the metal-assisted growth of III-V nanowires: Axial and radial growths, *J. Appl. Phys.* **105**, 114304 (2009).
- [66] F. Oehler, A. Cattoni, A. Scaccabarozzi, G. Patriarche, F. Glas, and J. C. Harmand, Measuring and modeling the growth dynamics of self-catalyzed GaP nanowire arrays, *Nano Lett.* **18**, 701 (2018).